DOI 10.1007/s11182-020-02089-1
Russian Physics Journal, Vol. 63, No. 5, September, 2020 (Russian Original No. 5, May, 2020)

CONDENSED-STATE PHYSICS

ADHESIVE PROPERTIES OF THE TiAl/Al_2O_3 INTERFACE

A. V. Bakulin,[1,2] S. S. Kulkov,[2] and S. E. Kulkova[1,2] UDC 538.915, 539.612, 544.14

*A systematic study of the atomic and electronic structure of the interface between the γ-*TiAl *alloy and α-*Al_2O_3*(0001) oxide depending on the contact configuration is performed within the density functional theory. The work of separation of the alloy film from the oxide surface is calculated for its various terminations. It is shown that high values of adhesion energy can be obtained at the interface with an* O*-termination of alumina due to the large ionic contribution to chemical bonding. An analysis of structural and electronic factors responsible for the decrease in adhesion at the interface with the metal oxide termination is performed. The calculation of the interfacial energy confirmed that the interface with the* O*-termination of alumina is energetically preferable.*

Keywords: interface, adhesion, chemical bonding, electronic structure, density functional theory.

INTRODUCTION

Composites based on metals/alloys and oxides have found an extensive application in present-day technologies attracting an increasing interest due to a feasibility of producing materials essentially differing in their properties from their components. Physical-chemical and mechanical properties of composites strongly depend on the characteristics of the oxide-metal interface controlled by their atomic and electronic structure. The knowledge of the electronic structure is necessary for gaining an insight into the nature of chemical bonding at the interfaces and the mechanisms for improving adhesion. Since the phenomena at the interfaces are critical for many engineering processes, they have been quite intensively studied within recent decades by a variety of methods, including the density functional theory, e.g., [1–13] and references in them. The largest number of works deal with the investigation of the Nb(111)/Al_2O_3(0001) interface, where a high adhesion energy of ~9.8–10.6 J/m^2 was found [2–5, 9, 11], and the interfaces between such fcc-metals as Al, Ni, Cu, Ag, Au, etc. and alumina [6–8, 10]. The focus of research is commonly on the interaction of individual atoms or metal monolayers with the oxide surface, which is important for understanding the mechanisms of metal film growth, but would not allow identifying the tendencies in the formation of stable interfaces. Furthermore, during oxidation of metals and alloys, oxide films are observed to grow on their surfaces. This prompts an investigation of the interaction of atomic or molecular oxygen with stable surfaces of metals and alloys, as this was done in a number of studies [14–18]. At present only a few studies are available, where the atomic and electronic structure and mechanical and thermodynamic properties of the alloy-oxide interfaces are discussed; most studies use α-Al_2O_3 oxide with the corundum structure [19–21]. Since the mechanism of chemical bonding at the interface is mainly determined by the electronic structure of alloys, a systematic comparative examination of the adhesive properties of interfaces within a single approach are necessary. The purpose of this work is to study the atomic and electronic structure of the TiAl(111)/Al_2O_3(0001) interface in dependence on the contact configuration and (0001) oxide surface termination.

[1]Institute of Strength Physics and Materials Science of the Siberian Branch of the Russian Academy of Sciences, Tomsk, Russia, e-mail: bakulin@ispms.tsc.ru; kulkova@ms.tsc.ru; [2]National Research Tomsk State University, Tomsk, Russia, e-mail: sskulkov@ispms.tsc.ru. Translated from Izvestiya Vysshikh Uchebnykh Zavedenii, Fizika, No. 5, pp. 3–9, May, 2020. Original article submitted February 12, 2020.

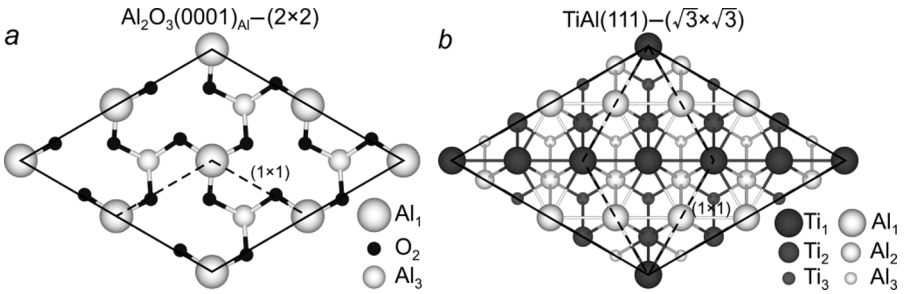

Fig. 1. Atomic structure of the $Al_2O_3(0001)_{Al}$ (*a*) and TiAl(111) (*b*) surface cells. Primitive cells (1×1) are shown by dashed lines.

CALCULATION PROCEDURE

The atomic and electronic structure of the TiAl(111)/Al_2O_3(0001) interface was calculated by the projector augmented wave method (PAW) in a plane-wave basis [22, 23] using a generalized approximation in the GGA-PBE form [24] for the exchange-correlation potential. The plane-wave cutoff energy was 550 eV. We used a Γ-centered grid of *k*-points 3×3×1. Relaxation of the atomic positions of interfacial layers was performed until the force per atom was ~0.01 eV/Å. The interface was simulated within the supercell approach using periodic boundary conditions. The method of thin films separated by a ~15 Å vacuum gap in a single-interface model was adopted. The theoretical lattice parameters of TiAl alloy (a = 3.977 Å and c = 4.081 Å) differ from the experimental values (a = 3.975 Å and c = 4.068 Å [25]) by ~0.3% only. The lattice parameters of α-Al_2O_3 (a = 4.808 Å and c = 13.118 Å) are also in a good agreement with the experimental data (a = 4.756 Å and c = 12.982 Å [26]), differing by ~1.0%. In simulating the interface we used the following surface cells: $Al_2O_3(0001)$ – (2×2) and TiAl(111) – (√3×√3)R30° (Fig. 1). This approach results in a mismatch in the parameters of the oxide and alloy surfaces (9.616 and 9.826 Å) which does not exceed ~2.2%. Note that every atomic layer of the alloy has a stoichiometric composition and is formed by six titanium and six aluminum atoms. The computational cell consists of 124 to 132 atoms, depending on whether the oxide terminates with oxygen or aluminum layer or two aluminum layers. In the calculations, the oxide lattice parameter was used, and the alloy lattice parameter was decreased by 2.1% in the plane of the interface but was increased in the perpendicular direction.

The work of separation (W_{sep}) or ideal adhesion energy were calculated via the formula

$$W_{sep} = \left(E^{slab}(Al_2O_3) + E^{slab}(TiAl) - E^{slab}(Al_2O_3/TiAl)\right)\Big/S, \quad (1)$$

where E^{slab}(TiAl/Al_2O_3) is the total energy of a supercell containing the alloy and oxide films, E^{slab}(TiAl) and E^{slab}(Al_2O_3) are the total energies of the supercells containing either the alloy or oxide only, S is the interface area.

The interfacial energy was estimated using the following formula:

$$\gamma = \sigma(TiAl) + \sigma(Al_2O_3) - W_{sep}, \quad (2)$$

where σ(TiAl) and σ(Al_2O_3) are the surface energies of the alloy and oxide, respectively. Since the TiAl(111) surface has a stoichiometric composition, its energy was calculated by a standard formula

$$\sigma_{TiAl} = \left(E^{slab} - NE^{bulk}\right)\Big/2S, \quad (3)$$

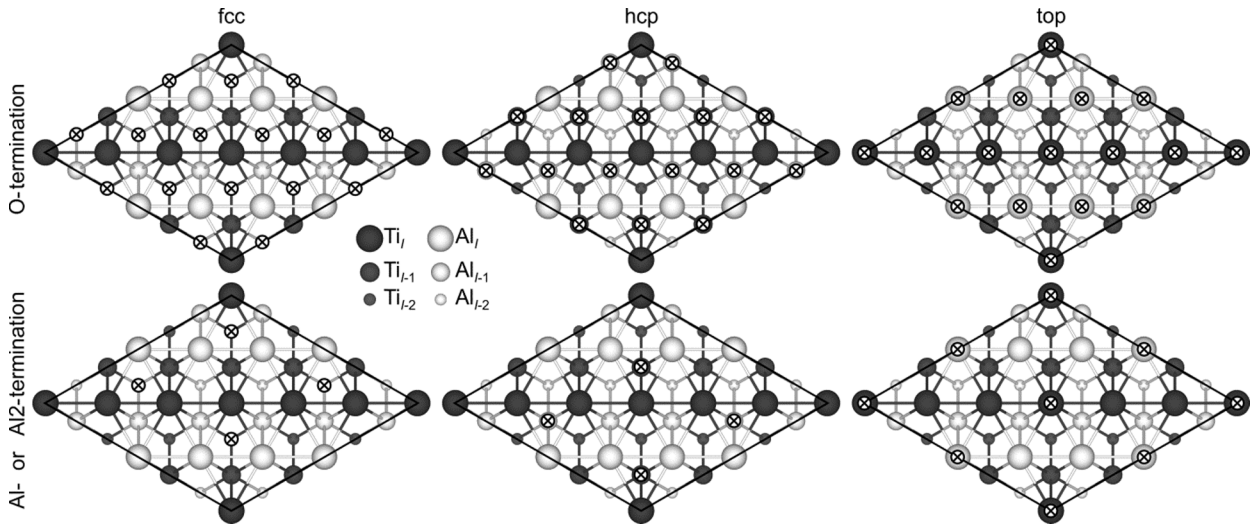

Fig. 2. Variants of contact at the $TiAl/Al_2O_3$ interface. Positions of interfacial oxide atoms are denoted by crosses.

where E^{slab} is the total energy of the supercell containing an alloy film, E^{bulk} is the bulk alloy energy calculated per formula unit, N is the number of formula units in the film, S is the surface area. Multiplier 2 is due to the presence of equal surfaces on both sides of the film.

The surface energy of a nonstoichiometric surface depends on chemical potentials of the components, so in the case of alumina a more complicated formula was used

$$\sigma_{Al_2O_3} = \left(E^{\text{slab}} - 1/2 N_{Al} E^{\text{bulk}}(Al_2O_3) - 1/2 E(O_2)\{N_O - 3/2 N_{Al}\} - \Delta\mu_O \{N_O - 3/2 N_{Al}\} \right) \Big/ 2S , \qquad (4)$$

where $\Delta\mu_O$ is the deviation from the chemical potential of oxygen on the surface of the oxide from its value in the gas phase. The law of energy conservation implies a restriction on its value: $1/3H^f \le \Delta\mu_O \le 0$, where H^f is the oxide formation energy equal to 16.82 eV.

RESULTS AND DISCUSSION

Three alloy-oxide contact configurations were simulated in this study for three possible oxide film terminations: fcc – where the oxide atoms occupy the positions above the atoms of the third alloy layer from the interface, hcp – where the interfacial atoms of the oxide are located above the atoms of the second interfacial layer of the alloy, and top – where the oxide atoms occupy the top positions above the atoms of the interfacial layer of the alloy (Fig. 2).

Table 1 demonstrates that the highest values of the work of separation have been obtained for the $TiAl(111)/Al_2O_3(0001)_O$ contacts having O-termination of the oxide, with the values of W_{sep} for the configurations under study being 0.7–1.2 J/m^2 larger than those at the $Al(111)/Al_2O_3(0001)_O$ interface [7]. At the same time, the presence of titanium in the interfacial layer does not change the most preferred configuration of the contact. Similarly to [7], irrespective of the oxide termination an fcc-configuration is the most preferred one. If the oxide terminates with an aluminum or double aluminum layer (Al- or Al2-terminated oxides), then the values of W_{sep} become considerably lower (Table 1).

On the whole, an analysis of the structure parameters demonstrated that a smaller interfacial distance corresponds to a larger work of separation. In a number of cases however (O-terminated hcp-configuration; Al-terminated hcp- and top-configurations), there is a considerable displacement of certain interfacial Ti atoms towards the

TABLE 1. The Work of Separation and Interfacial Distance at the TiAl(111)/Al_2O_3(0001) and Al(111)/Al_2O_3(0001) Interfaces (in Brackets) [7]

Contact configuration	W_{sep}, J/m^2			Contact configuration	d, Å		
	Al_2O_3(0001)-termination				Al_2O_3(0001)-termination		
	O	Al2	Al		O	Al2	Al
fcc	10.43 (9.73)	2.68	1.19 (1.06)	fcc	1.33 (0.86)	2.23	2.16 (0.70)
hcp	10.15 (9.11)	2.58	1.12 (0.41)	hcp	1.36 (1.06)	2.25	2.60 (2.57)
top	9.97 (8.75)	2.27	1.08 (0.84)	top	1.77 (2.00)	2.78	2.56 (1.62)

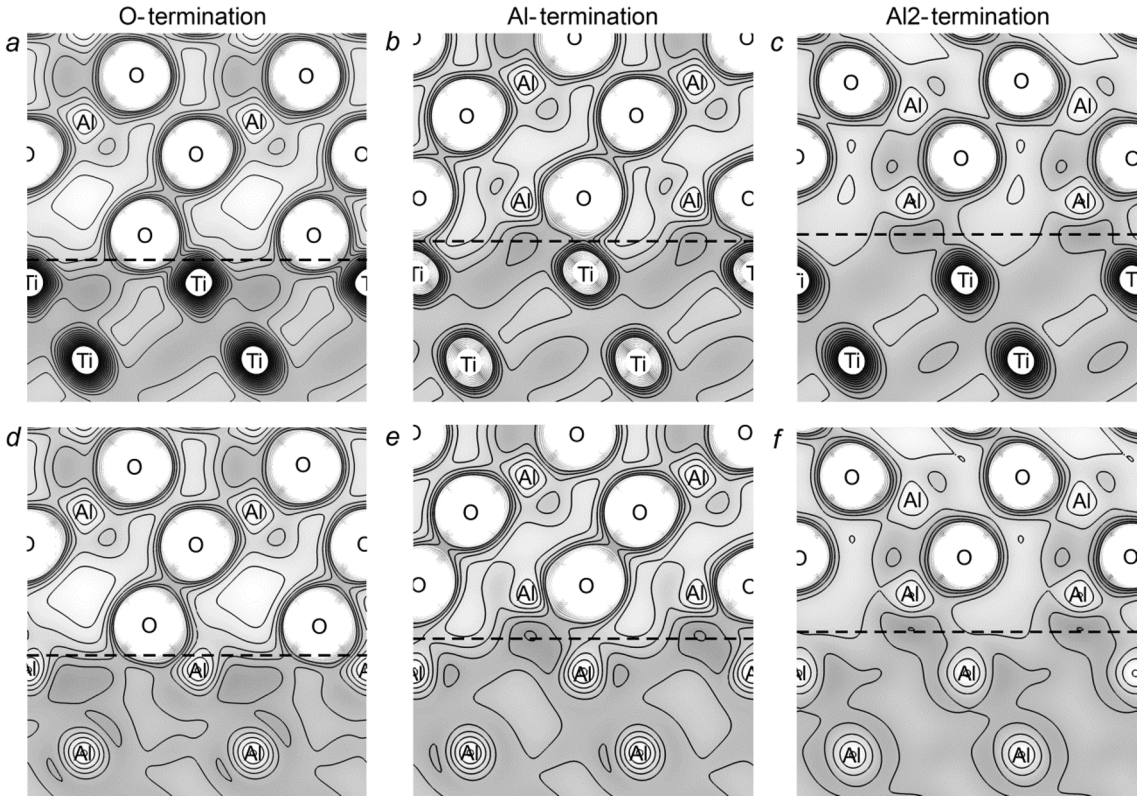

Fig. 3. Total charge density distribution for three types of termination of the Al_2O_3(0001) surface and most stable fcc-configurations of the TiAl/Al_2O_3 interface in the planes passing through the interfacial atoms of the alloy: titanium (*a*, *b*, *c*) and aluminum (*d*, *e*, *f*). Dashed line indicates the interface location.

oxide. Since formally this gives rise to a decrease in the interfacial distance, Table 1 lists the values calculated from the average positions of the interfacial layer atoms. Note in this case that, according to the calculation of the overlap population, the interaction (chemical contribution into the work of separation) enhances between the individual interfacial atoms only, while the mechanical contribution responsible for a weaker interaction increases to a higher degree. Decomposition of the work of separation into separate contributions is detailed elsewhere [27, 28]. A competition between these two contributions results in a somewhat lower work of separation values for these configurations (Table 1).

The total charge-density distribution given in Fig. 3 allows demonstrating the features of interaction between the interfacial atoms for different oxide terminations in the cases of the most preferred fcc-configurations. It is clear in Fig. 3*a* that at the interface with the O-terminated oxide the O–Ti bond has an ionic-covalent character, while the O–Al

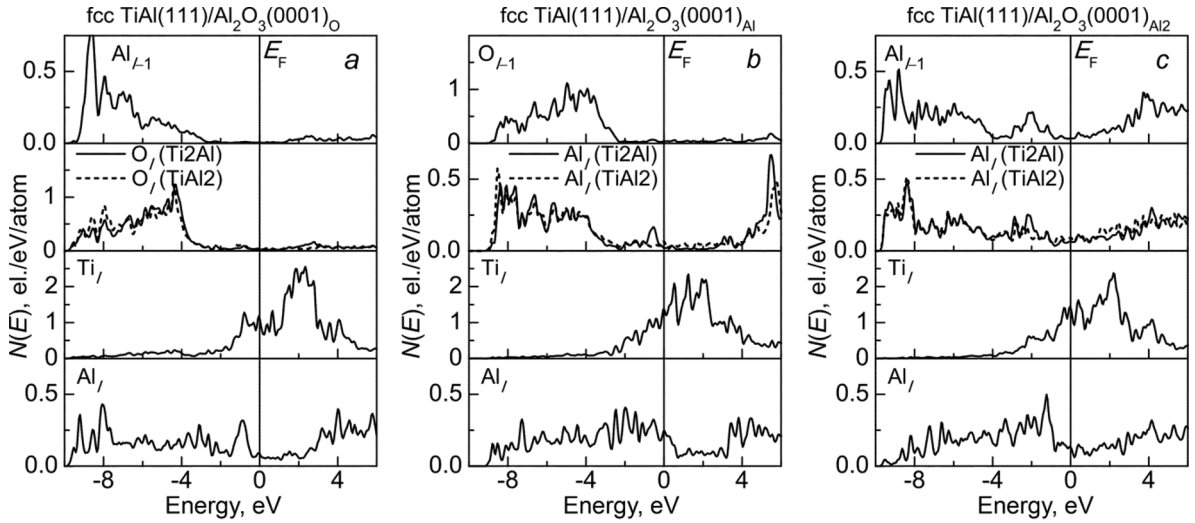

Fig. 4. Local densities of electronic states of interfacial Ti, Al and O atoms for three terminations of the $Al_2O_3(0001)$ surface and most stable fcc-configuration of the $TiAl/Al_2O_3$ interface.

bond is predominantly ionic (Fig. 3*d*). This difference is due to different nature of the valence states of titanium and aluminum: *d*-electrons are strongly localized, which determines the increased covalence of atomic bonding of the transition metals, in particular Ti, with the electronegative elements, while *s*, *p*-states of Al atoms are readily involved into interaction with oxygen and participate in the formation of ionic bonding. In the case of an interface with an Al-terminated oxide surface, bonding between the interfacial Al–Ti and Al–Al atoms is mostly of metallic character, which is quite evident in Fig. 3*b* and *e* from the weak localization of the electronic density on the interatomic bonds. It should be noted that there is also interaction of the interfacial atoms of the alloy with the oxygen atoms of the second layer from the interface. The character of this bonding remains the same as in the previous case, though the strength is noticeably weaker, which is clear from the decreased number of isolines. Finally, at the interface with the Al2-terminated oxide (Fig. 3*c* and *f*) interaction between the interfacial atoms is mostly of metallic character also. Note that the formation of bonds with the oxygen atoms of the second layer in the case of an interface with the Al-terminated oxide favors a decrease in the interfacial distance compared to that with the Al2-terminated oxide.

Figure 4 presents the local densities of electronic states (DOS) of the oxide and alloy interfacial atoms for the interfaces discussed above. It is seen in Fig. 4a that in the case of the O-terminated oxide and fcc-configuration there is a strong hybridization of the oxygen states both with *s*, *p*-states of aluminum atoms and with *d*-states of titanium atoms of the interfacial layer. It has to be noted that six out of twelve interfacial oxygen atoms are located practically above the centers of the triangles formed by two titanium and one aluminum atoms (Ti2Al), while the remaining six atoms – above the TiAl2 triangles. The density of electronic states of the latter oxygen atoms is characterized by higher peaks localized at the energies –8.6 eV and –8.0 eV corresponding to the sharp DOS peaks of aluminum in the interfacial layer of the alloy. At the energies from –7.0 to –3.3 eV, where the split-off low-lying titanium states are located, a higher density of states of oxygen bound with two titanium atoms is observed (Fig. 4*a*). As noted earlier, *s*, *p*-states of aluminum are more readily involved into interaction than are *d*-states of titanium, therefore these states are much stronger displaced towards negative energies, which accounts for the above-noted peculiarities of DOS of oxygen atoms. It is evident from Fig. 4*a* that at the O-termination of this interface there is partial depletion of states of titanium atoms, which is expressed much stronger, compared to other terminations (Fig. 4*b* and *c*). The latter circumstance indicates a large ionic contribution into chemical bonding at the $TiAl(111)/Al_2O_3(0001)_O$ interface. The results of the charge transfer calculations show that the interfacial titanium atoms lose ~0.5 electrons. The local DOSs of aluminum

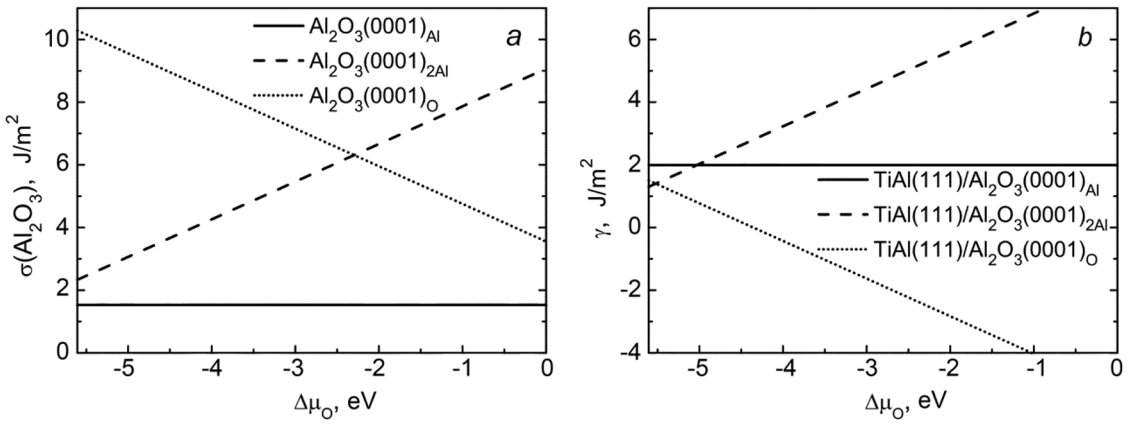

Fig. 5. Surface energy of $Al_2O_3(0001)$ (*a*) and interfacial energy of the Ti_3Al/Al_2O_3 interface (*b*) as a function of termination of the $Al_2O_3(0001)$ surface and chemical potential of oxygen. The results are given for fcc-configurations of interfaces.

atoms of the second oxide layer vary not so much as do the DOSs of aluminum atoms in the bulk, which indicates their weak involvement into interaction with the alloy atoms.

In the case of an Al-terminated oxide, there is also a good agreement of the fine structure of DOS of the oxide and alloy interfacial atoms, though titanium atoms are involved into interaction much weaker than aluminum atoms (Fig. 4*b*). It should be noted that similarly to the previous case half of the interfacial atoms of the oxide are located above the centers of the Ti2Al triangles, and the second half – above the TiAl2 triangles. This gives rise to insignificant differences between DOSs of Al_I (Ti2Al) and Al_I (TiAl2) atoms, shown in Fig. 4*b*. Despite the interaction between the oxygen atoms of the second layer from the interface and the interfacial titanium and aluminum atoms (the latter can be seen from the agreement of the positions of DOS peaks of O_{I-1} and Al_I atoms in Fig. 4*b*), weak metallic Al–Al- and Al–Ti-bonds at the interface result in a much lower work of separation. In the case of an Al2-terminated oxide there is hybridization of *s*, *p*-states of aluminum atoms of the *I*- and *I*–1-layers with the states of titanium and aluminum atoms of the alloy, which favors an increase in the work of separation at the interface compared to the Al-terminated oxide. A similar increase in adhesion also takes place at the interfaces between transition metals and alumina [6, 8, 10]. In general, the resulting DOSs support the conclusions obtained from the analysis of the total charge density distributions.

Figure 5 presents the surface and interfacial energies of the systems under study calculated as a function of the chemical potential of oxygen. According to formula (2), a lower interfacial energy corresponds to a larger work of separation. It is evident from Fig. 5*b* that the $TiAl(111)/Al_2O_3(0001)_O$ interface is stable practically in the entire interval of variation of the oxygen chemical potential. Only in the limit of low oxygen concentration the interface with an Al2-terminated oxide becomes stable. At $\Delta\mu_0 > -4.4$ eV, the interfacial energy becomes negative, which indicates an energy preference of oxygen segregation towards the $TiAl(111)/Al_2O_3(0001)$ interface.

An increased titanium content in the alloy gives rise to stronger adhesion, as shown in [21], where the authors studied the $Ti_3Al/Al_2O_3(0001)$ interface, which is determined by stronger interaction of *d*-states of titanium with 2*p*-states of oxygen compared with the interaction of *s*, *p*-orbitals of aluminum with oxygen. The influence of impurities only slightly decreases the adhesion energy at this interface [21]. One can hope that the influence of impurities would be similar in the case of the $TiAl(111)/Al_2O_3(0001)$ interface. Their influence on the interface morphology might be stronger, since according to [29, 30], impurities can destabilize Al_2O_3 and give rise to the formation of a $TiAl/TiO_2$ interface.

SUMMARY

To sum up, a systematic study of the atomic and electronic structure of the TiAl(111)/Al_2O_3(0001) interface as a function of the contact configuration and oxide surface termination has been performed. For the interface of a nonstoichiometric composition corresponding to the (0001) oxygen-terminated polar surface of alumina and TiAl alloy larger values of adhesion have been obtained than for the oxide terminated with metal. A correlation has been observed for all interfaces under study between the electronic and structural factors and mechanical properties. Stability of the fcc-configuration at the oxygen-terminated interface is due to the large ionic contribution to the bonding mechanism, which results from the charge transfer from interfacial atoms of the alloy to oxygen. In the latter case, the least interfacial distance is observed between metallic and oxygen layers; this in turn favors strong hybridization of the metal and oxygen orbitals. The adhesion energy at the aluminum termination of the oxide is observed to be essentially lower, which is due to a weaker interaction between the metal atoms of the alloy and oxygen due to a larger distance between the alloy interfacial atoms and the oxygen in the oxide. Moreover, the interaction of aluminum with the interfacial atoms of the alloy gives rise to the restoration of bonding in the bulk oxide. In this case, the major chemical bonding mechanism is hybridization of orbitals of interfacial atoms of the alloy and aluminum. For the aluminum-enriched interface, metallic bonding predominates. On the whole, the results evidence of the importance of the ionic-covalence component in chemical bonding for achieving high adhesion at the alloy – oxide interface, as is the case with films of *d*-metals.

This study has been performed according to the Government research assignment for ISPMS SB RAS, Project No. III.23.2.8. The numerical calculations were performed at the SKIF-Cyberia supercomputer at Tomsk state university.

REFERENCES

1. J. T. Klomp, Surfaces and Interfaces of Ceramic Materials (Eds. L. C. Dufour, C. Monty, and G. Petot-Ervas), Kluwer Academic Publ., Dordrecht (1989).
2. M. W. Finnis, J. Phys.: Cond. Matter., **8**, 5811–5836 (1996).
3. C. Kruse, M. W. Finnis, J. S. Lin, *et al*., Philos. Mag. Lett., **73**, 377–383 (1996).
4. I. G. Batirev, A. Alavi, M. W. Finnis, *et al*., Phys. Rev. Lett., **82**, 1510–1513 (1999).
5. W. Zhang and J. R. Smith, Phys. Rev. B, **61**, 16883–16889 (2000).
6. W. Zhang and J. R. Smith, Phys. Rev. Lett., **85,** 3225–3228 (2000).
7. D. J. Siegel, L. G. Hector, and J. B. Adams, Phys. Rev. B, 65, 085415-1–19 (2002).
8. J. Feng, W. Zhang, and W. Jiang, Phys. Rev. B, **72**, 115423-1–11 (2005).
9. S. V. Eremeev, L. Yu. Nemirovich-Danchenko, and S. E. Kulkova, Phys. Solid State, 50, Iss. 3, 543–552 (2008).
10. S. E. Kulkova, S. V. Eremeev, S. Hocker, *et al*., Phys. Solid State, **52**, Iss. 12, 2589–2595 (2010).
11. V. V. Melnikov and S. E. Kulkova, JETP, **114**, Iss. 2, 305–313 (2012).
12. S. E. Kulkova, A.V. Bakulin, S. Hocker, S. Schmauder, Technical Physics, **58**, Iss. 3, 325–334 (2013).
13. S. Hocker, S. Schmauder, A. Bakulin, *et al*., Philos. Mag., **94**, 265–284 (2014).
14. M. Nolan and S.A.M. Tofail, Biomaterials, **31**, 3439–3448 (2010).
15. S. E. Kulkova, A. V. Bakulin, Q. M. Hu, *et al*., Physica B, **426**, 118–126 (2013).
16. S. Y. Liu, S. Liu, D. Li, *et al*., Phys. Chem. Chem. Phys., **14**, 11160–11166 (2012).
17. A. V. Bakulin, S. Hocker, S. Schmauder, *et al*., Appl. Surf. Sci., **487**, 898–906 (2020).
18. S. E. Kulkova, A. V. Bakulin, and S. S. Kulkov, Comput. Mater. Sci., **170**, 109136-1–9 (2019).
19. Y. M. Ni, R. T. Wu, R. C. Reed, *et al*., Mater. Res. Innov., **18**, S2-1001–1007 (2014).
20. Z. Zhang, R. F. Zhang, D. Legut, *et al*., Phys. Chem. Chem. Phys., **18,** 22864– 22873 (2016).
21. A. V. Bakulin, A. A. Fuks, and S. E. Kulkova, AIP Conf. Proc., **2167**, 020027-1–4 (2019).
22. P. E. Blöchl, Phys. Rev. B, **50**, 17953–17979 (1994).
23. S. Kresse and J. Joubert, Phys. Rev. B, **59**, 1758–1775 (1999).

24. J. P. Perdew, K. Burke, and M. Ernzerhof, Phys. Rev. Lett., **77**, 3865–3868 (1996).
25. K. Tanaka, T. Ichitsubo, H. Inui, *et al*., Philos. Mag. Lett., **73**, 71–78 (1996).
26. M. Lucht, M. Lerche, H. C. Wille, *et al*., J. Appl. Crystallogr., **36**, 1075–1081 (2003).
27. A. Y. Lozovoi, A. T. Paxton, and M. W. Finnis, Phys. Rev. Lett., **74**, 155416-1–13 (2006).
28. S. S. Kulkov, A. V. Bakulin, and S. E. Kulkova, Int. J. Hydrogen Energy, **43**, 1909–1925 (2018).
29. F. P. Ping, Q. M. Hu, A. V. Bakulin, *et al*., Intermetallics, **68**, 57–62 (2016).
30. P. Zhao, X. Li, H. Tang, *et al*., Oxid. Met. (2020). https://doi.org/10.1007/s11085-020-09964-9.